Electronic Structure of $Ag_2Cu_2O_4$. Evidence of Oxidized Silver and Copper and Internal Charge Delocalization

D. Muñoz-Rojas,† G. Subías,‡ J. Fraxedas,† P. Gómez-Romero,† and N. Casañ-Pastor*,†

Institut de Ciencia de materials de Barcelona, CSIC, Campus UAB, 08193 Bellaterra, Barcelona, Spain, and Instituto de Ciencia de Materiales de Aragón, CSIC−Universidad de Zaragoza, Pza. San Francisco s/n, 50009-Zaragoza, Spain

Received: December 3, 2004; In Final Form: February 4, 2005

The electronic structure of the recently isolated silver copper oxide $Ag_2Cu_2O_4$ is analyzed along with its precursor $Ag_2Cu_2O_3$ and similar binary oxides, Ag_2O, AgO, CuO, and $NaCuO_2$, using X-ray photoemission (XPS) and X-ray absorption (XAS) measurements. The results for $Ag_2Cu_2O_4$ reveal an electronic distribution in which silver and copper share a delocalized valence scheme with both metals in formal oxidation states larger than the usual Ag^I and Cu^{II}. Only one type of crystallographic silver or copper is found, but disorder−strain parameters are considerable and the possibilities of thermal disorder, atomic motion, oxygen contribution, mixed valence, and internal charge delocalization are considered. Classical coordination descriptions for oxidized silver are revisited in terms of this new internal charge delocalization framework found for the electronic structure.

Introduction

Silver and copper are frequently found together in alloys and some ternary compounds, namely sulfides, selenides, and tellurides.[1] However, the first oxide containing both elements, $Ag_2Cu_2O_3$, was synthesized and reported only recently.[2−4] This new oxide was prepared by coprecipitation and aging at room-temperature in alkaline aqueous media or at relatively low temperatures (up to 125 °C, in molten hydroxides). Preparing a silver-containing cuprate superconductor has been an ambitious goal in worldwide laboratories inspired by the high T_c mercury-based superconductors, but that objective has remained elusive. Moreover, other silver copper oxides have been obtained by doping of the silver−lead oxide,[5] leading to a solid solution of formula $Ag_5Pb_{2-x}Cu_xO_6$ ($0 \le x \le 0.5$). In all those cases the formal oxidation states are Ag^I and Cu^{II} for the metals and indeed the charges match those of oxygen considered as O^{2-}. Doping the existing silver copper oxide, $Ag_2Cu_2O_3$, either by cation substitution or oxygen intercalation was one of the rational approaches in order to achieve a metallic mixed valence system that may present electro-activity or interesting transport properties. Both silver and copper are known to form compounds with high formal oxidation states, namely Ag^{III} [6] (Ag^{II} reported in fluorides[7,8]) and Cu^{III}.[9,10] Furthermore, the chemistry of high-valent cuprates, exemplified by high T_c phases, has shown the very likely involvement of oxygen in delocalization of positive charge customarily assigned to metals.

This paper relates to a phase recently obtained by oxygen insertion into $Ag_2Cu_2O_3$.[11−13] The open channel structure observed for $Ag_2Cu_2O_3$ and the possibility of various oxidation states for both metals suggested the possibility of redox intercalation reactions (see Figure 1). In particular electrochemical oxidation of $Ag_2Cu_2O_3$ has allowed intercalation of oxygen but with a final change in structure to $Ag_2Cu_2O_4$ (see Figure 2) with an extra oxygen atom per unit formula (this formula can be simplified to the empirical $AgCuO_2$). Chemical oxidation is also possible from the same precursor[14] and also from solutions[15] or from suspensions of the simple solid metals or oxides.[11−13,16] However, we will maintain the double formula for those

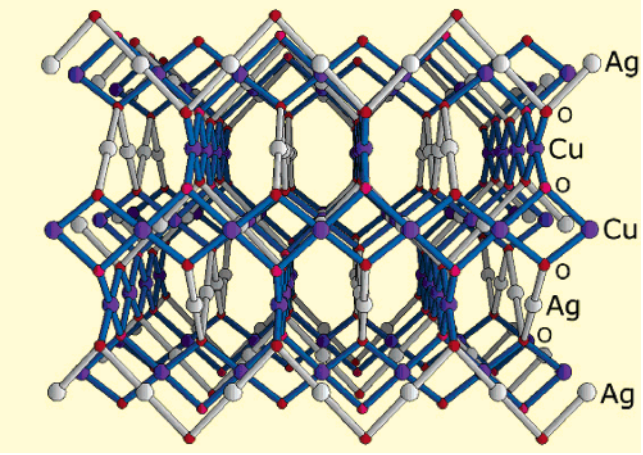

Figure 1. Refined structure for $Ag_2Cu_2O_3$.[3]

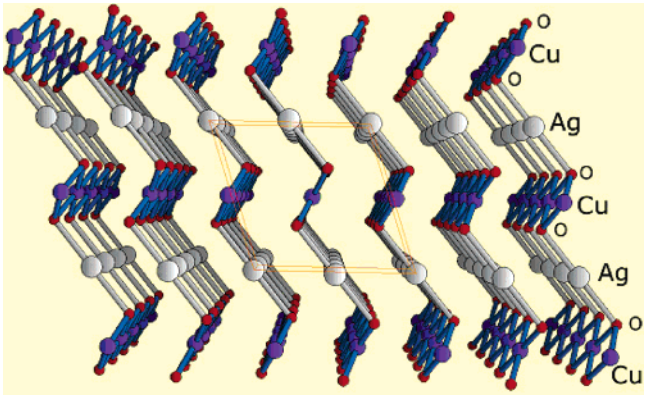

Figure 2. Refined structure for $Ag_2Cu_2O_4$, from refs 12 and 13.

† Institut de Ciencia de Materials de Barcelona, CSIC, Campus UAB.
‡ Instituto de Ciencia de Materiales de Aragón, CSIC−Universidad de Zaragoza.
* Corresponding author. E-mail: nieves@icmab.es.

10.1021/jp044493w CCC: $30.25
Published on Web 03/15/2005

obtained from suspensions and the empirical formula for those obtained by oxidation of solutions. The electrochemical synthesis procedure represents a substantial modification of other previously reported low-temperature oxygen intercalation in pellets of oxides with structure related to perovskite, such as $SrFeO_{2.5}$, La_2NiO_4, La_2CuO_4[10,17−21] and $Ca_{2-x}Ln_xMnO_4$, or $Ln_2Ba_2Cu_2Ti_2O_{11}$[22,23] in aqueous and nonaqueous media.[20,22,23] In previous cases, oxidation of an oxide pellet acting as electrode was carried out. The present modification consists of the oxidation of a suspension instead of an oxide pellet, a most useful procedure in phases that cannot be sintered such as silver oxides, and it constitutes by itself a breakthrough in the synthesis of new oxides by soft methods.

In fact, preliminary cyclic voltammetry experiments showed that the phase was electroactive with reduction and oxidation waves that could allow the synthesis of new phases either by reduction or oxidation.[20,24] Electrochemical reduction has been reported to yield Ag and Cu_2O (and eventually Cu) that upon reoxidation yield CuO and Ag_2O in aqueous alkaline media.[20,24] Oxidation in acetonitrile, a medium with no free oxygen species, apparently involves silver, copper, and oxygen deintercalation[25] with decomposition and without the isolation of any new phase or solid solution. On the other hand, if oxidation of $Ag_2Cu_2O_3$ is carried out in an aqueous alkaline media, a new phase is observed upon electrolysis at $E > 0.42$ V, a phase written here with the formula $Ag_2Cu_2O_4$.[11−13]

The structural refinements for $Ag_2Cu_2O_4$, obtained by electrochemical oxidation from $Ag_2Cu_2O_3$,[11−13] based on electron diffraction "reconstructions" and X-ray powder diffraction and those of simultaneously reported $AgCuO_2$,[15] showed that both phases are essentially the same in terms of diffraction pattern, although the crystallization is better for the electrochemical phase. Authors in ref 15 suggested that $AgCuO_2$ could be described with the structure of AgO,[26] represented by the formula $Ag^IAg^{III}O_2$, where copper would occupy the Ag^{III} square planar position and silver the Ag^I position in AgO. That involves the underlying assumption that copper assumes the role of the +3 ion while silver remains as the +1 ion or the assumption that it is easier to oxidize copper than silver. The refinement yields only one type of crystallographic silver or copper, and therefore it seems to support the previous assumption. However, it also involves the assumption that a single silver, formally Ag^{II}, cannot exist and that it will always disproportionate into Ag^I and Ag^{III}. That point has been considered traditionally true for oxides although not for fluorides.[7,8] In any case, both refinements reported[13,15] need only a single type of silver metal and copper metal to refine the structure with satisfactory statistical parameters. The statistics are good especially for the better crystallized electrochemical phase, but both space groups tested $P2_1/c$ or $C2/m$ present many special atomic positions and allow refinement of only two out of the nine atomic coordinates.

According to these data, assuming that oxidation would localize at the copper, the final phase, $AgCuO_2$, would contain Ag^I and Cu^{III}. However, XPS experiments reported in 2002[12,13] were indicating a more complex case. First, they showed extra components for the Ag 3d spin−orbit lines, in contrast with the well-defined single components of the $Ag_2Cu_2O_3$ phase, and no significant change in the Cu 2p signals. This observation could be easily taken, according to the knowledge on silver oxides, as an evidence of an additional localized oxidation state for silver[26] and therefore of silver oxidation. Even though it seemed unusual to be finding oxidized silver instead of oxidized copper, the phase could be tentatively described by the doubled formula, $Ag^IAg^{III}Cu_2^{II}O_4$, which would contain mixed-valence silver. Indeed, although first ionization potentials predict copper to be more easily oxidized than silver, if the calculation takes into account up to the third potential the prediction is inverted.[12] If that is so, however, two types of structural silver ions are expected instead of the one derived from the refinement, and finding only one could be due to atomic disorder, while a new description of the phase may also be needed.

Therefore, XPS opened up a new possible interpretation, and also an apparent contradiction, for what turns out to be a complex phase, $Ag_2Cu_2O_4$, with an unusual charge distribution among metals Cu and Ag and possibly structural disorder. On the other hand, since XPS may be showing a dominant contribution from the surface (even in these small nanosized particles where the amount of material observed for the silver signal is rather large, see ref 14), this work attempts to elucidate additional aspects of the electronic structure of the material, by studying it with complementary local probes affecting the bulk material, as X-ray absorption near-edge (XANES) and Extended X-ray absorption fine structure (EXAFS) spectroscopy. Those spectroscopic techniques, used successfully before for Ag (L and K edges) and Cu (K edge),[27−29] yield information about oxidation states, delocalization vs localization schemes and local structures of the bulk phase, while their temperature dependence may be defining additional order/disorder factors. Within this new frame, additional XPS data also gives a different perspective of these oxides.

Experimental Section

$Ag_2Cu_2O_3$ was synthesized as previously described.[2−4] Equimolar amounts (3.2 mmol) of $CuNO_3 \cdot 3H_2O$ (Merck, p.a. 99.5%) and Ag_2NO_3 (Panreac, p.a., 99.98%) were dissolved in 2 mL of water, and the solution was then poured into 4 mL of a 3 M NaOH solution, while stirring vigorously. A dark-green precipitate formed. The precipitate was kept in suspension during 12 h with continuous stirring. The dark solid was then vacuum-filtered, washed and dried. Electrochemical oxidation of the oxide $Ag_2Cu_2O_3$ was performed in alkaline media in the conditions described in ref 12. A stirred suspension of $Ag_2Cu_2O_3$ in a 1 M NaOH solution was used and the experiments were carried out in a three-electrode cell. A platinum foil (1 cm^2) was used as working electrode; platinum wires (1 mm diameter) were used as pseudo-reference electrode and counter electrode, respectively. The counter electrode was placed in a separate half cell, connected to the other half cell by glass fritted membrane to avoid direct contact with the suspension. The experiments were controlled using a McPile II, BioLogic Science Instruments galvanostat/potentiostat. Completion of the reaction was determined by taking aliquots periodically and performing powder X-ray diffraction experiments, until no changes were observed. No intermediate phases were observed. The same product was also obtained by oxidation of Ag + Cu or Ag_2O + CuO suspensions.[16] $Ag_2Cu_2O_4$ was also synthesized by chemical oxidation using sodium persulfate (1.5 g in 30 mL 10% aqueous KOH) as oxidizing agent on alkaline solutions containing the stoichiometric amounts of $AgNO_3$ and $Cu(NO_3)_2 \cdot 2H_2O$ as in ref 30 (this phase is named $AgCuO_2$ throughout the paper) and by oxidation of $Ag_2Cu_2O_3$ with ozone as in ref 14. The ozone treated sample shows oxygen over-stoichiometry (4.33 instead of 4.00).

AgO (Aldrich, 99.9%), Ag_2O (Panreac, pure), and CuO (Aldrich, 99.99%) were used as purchased. $NaCuO_2$ was synthesized electrochemically by oxidation from fused hydroxides, according to the procedure described in ref 31. The identity of all phases was checked by X-ray powder diffraction. The

products obtained by chemical oxidation were analyzed in various ways. X-ray powder diffraction data was collected using a Rigaku X-ray powder diffractometer "Rotaflex" Ru-200B, $10 < 2\theta < 90°$, step 0.02°, radiation Cu $K\alpha_1$. Atomic absorption spectroscopy was used to determine the stoichiometry of Ag and Cu in the oxidized and precursor compounds. The oxygen content was evaluated by TGA analysis in Ar/H_2 (5%) atmosphere at 600 °C (flow rate of 75 cm^3/min, heating rate of 2 °C/min + isotherm) on a Perkin-Elmer TGA 7 thermal balance. (Final products in this analysis are metallic Ag and Cu as confirmed by X-ray diffraction.) The analysis of the crystal morphology and size was performed using a scanning electron microscope JEOL JSM-6400 and JSM-6300 (JEOL Ltd. Tokyo, Japan), with EDX analysis also performed. XPS measurements were performed at room temperature with a SPECS EA10P hemispherical analyzer using both nonmonochromatic Mg Kα (1253.6 eV) and Al Kα (1486.6 eV) radiation as excitation source in a base pressure of $\approx 10^{-9}$ mbar, on pressed pellets, avoiding to use silver epoxy. The Ag 3d signal is measured at the start and the end of the experiment to check for possible degradation. None has ever been observed. XANES and EXAFS measurements were performed at beamline BM29[32] of the European Synchrotron Radiation Facility. A fixed-exit Si(311) double-crystal monochromator was used, with estimated resolutions being $\Delta E/E = 8 \times 10^{-5}$ at Ag K-edge and 7×10^{-5} at Cu K-edge, respectively. Harmonic rejection was achieved by 50% (Cu−K) or 30% (Ag−K) detuning of the two crystals from the parallel alignment. Absorption spectra ($30\ K \leq T \leq 300\ K$) were recorded in the transmission mode using ionization chambers as detectors on pellets prepared with BN containing 50% of sample material for Ag K and 20% for Cu K edges in order to optimize the thickness. Simultaneously, a Ag or Cu metal foil at Ag K-edge or Cu K-edge, respectively, was measured for energy calibration. No visible signs of decomposition, or metallic silver, were observed in situ or later by X-ray diffraction.

XANES spectra were normalized to the high part of the spectrum (≈100 eV above the absorption edge) after linear background subtraction.[33] EXAFS $\chi(k)$ spectra were obtained by removing the smooth atomic absorption coefficient, μ_0, by means of a cubic spline fit. The structural analysis was performed in the R-space fitting mode including multiple scattering terms up to 4 Å (first and second coordination shells) using the FEFF 8.10 package.[34] Theoretical amplitudes and phases were calculated with the FEFF 8.10 code according to structural models obtained from the crystallography. The model used includes Gaussian distributions for Ag(Cu)−O, Ag−Ag, Ag(Cu)−Cu(Ag), and Cu−Cu paths, respectively.

Ionic conductivity studies were attempted but resulted in sample deterioration.

Results and Discussion

Figures 1 and 2 show the structures of the $Ag_2Cu_2O_3$ and $Ag_2Cu_2O_4$ phases, studied in this work as refined by X-ray and neutron powder diffraction data, respectively.[3,13] Several unit cells have been shown to draw attention to the type of silver and copper ordering in both frameworks. AgO was originally used as model to refine the structure of $AgCuO_2$[15] and has a structure of the same type, AgO interpreted as being $Ag^IAg^{III}O_2$, where there is a linear Ag^I and a square planar Ag^{III} (the positions equivalent to Cu in $AgCuO_2$).

XPS. Systematic XPS measurements have been performed on the samples discussed here using the same experimental conditions (pass energy, multiplier voltage, source power, etc.)

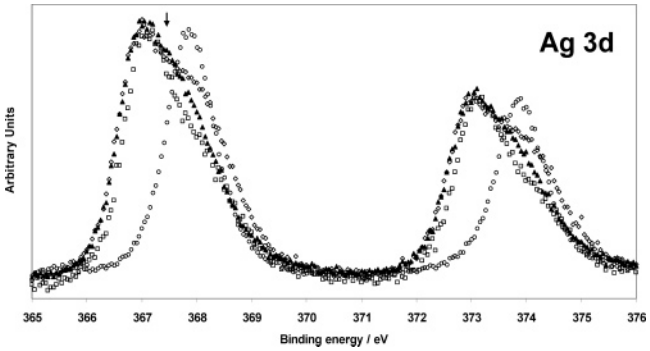

Figure 3. Ag XPS for the Ag 3d region for $Ag_2Cu_2O_3$ (○), $Ag_2Cu_2O_4$ (electrochemical; ◇), $Ag_2Cu_2O_{4.33}$ (oxidized with ozone; □), and $AgCuO_2$ (chemical $Ag_2Cu_2O_4$; ▲); ↓: AgO max.[35−38]

TABLE 1: XPS Binding Energies (eV) of Ag $3d_{5/2}$, O 1s, and Cu $2p_{3/2}$ Core Levels

	Ag $3d_{5/2}$	O 1s	Cu $2p_{3/2}$
Ag	368.1[35]		
	368.0[36]		
	368.0[37]		
Ag_2O	367.7[35]	529.0, 530.4[35]	
	367.5[36]	529.0, 530.8[36]	
	367.6[37]	528.9[37]	
		529.1, 530.5[39]	
$Ag_2Cu_2O_3$	367.9	529.1, 530.8, 532.4	933.0
AgO	367.4[35]	528.4, 530.3[35]	
	367.1[36]	528.3, 530.5[36]	
	367.3[37]	528.5[37]	
	367.4[38]	528.6[38]	
$Ag_7O_8NO_3$	367.4[36]	528.6, 531.6[36]	
$Ag_2Cu_2O_4$	367.0, 368.0	528.6, 530.7, 532.7	932.9

for each XPS line. Figure 3 shows the XPS spectra of the Ag 3d region for $Ag_2Cu_2O_3$ and $Ag_2Cu_2O_4$, prepared in various ways. We have included a sign where reported AgO appears. For the sake of comparison we will maintain the different formula, $AgCuO_2$ and $Ag_2Cu_2O_4$, as given before. No charging effects are observed in any of the samples mounted in the sample holder in various ways. The use of silver epoxy has been avoided because of the presence of silver.

The Ag 3d region of the spectrum consists of a spin−orbit coupling doublet, Ag $3d_{3/2}$ and Ag $3d_{5/2}$. Each peak presents a single component for $Ag_2Cu_2O_3$ (empty circles in Figure 3), with binding energies of 367.9 eV for the Ag $3d_{5/2}$ and 373.9 eV for the Ag $3d_{3/2}$ that corresponds to the Ag^I oxidation state (see comparison with Ag_2O in Table 1 and references therein). The spin−orbit splitting is 6.0 eV and the fwhm (full width at half-maximum) of the Ag $3d_{5/2}$ line is 1.1 eV. Earlier XPS measurements performed on AgO[35−39] and $Ag_7O_8NO_3$,[36] assumed to exhibit both Ag^I and Ag^{III} oxidation states, show broader and slightly asymmetric Ag 3d single lines shifted toward lower binding energies in smaller extent and without resolved components. Our observations on AgO (not shown) agree with those reported earlier.[35−38] The main Ag $3d_{5/2}$ peak is found at 367.4 eV and exhibits a fwhm of 1.7 eV, considerably larger than that for $Ag_2Cu_2O_3$, which we ascribe to unresolved components from both oxidation states.

On the other hand, the Ag $3d_{5/2}$ line in both types of $Ag_2Cu_2O_4$ (empty diamonds and triangles in Figure 3) exhibit one main component, at 367.0 and a shoulder at 368.0 eV, respectively, centered at energies even lower than the one found for AgO. The 367.0 and 368.0 eV components were tentatively assigned to specific localized oxidation states for silver, Ag^I and Ag^{III} respectively, in analogy with the AgO structure. The formula could then be written as $Ag^IAg^{III}Cu^{II}_2O_4$ in terms of classical formal oxidation states that imply oxidation of the

SCHEME 1: Photoionization for Different Integer Electron Configurations in the Ag 3d XPS Region (L Stands for Ligand Holes)[a]

$$Ag^{I}\ d^{10}\ \text{closed shell}: |3d^{10}4d^{10}> \rightarrow |3d^{9}4d^{10}>$$

$$Ag^{II}\ d^{9}: |3d^{10}4d^{9}> \rightarrow \alpha|3d^{9}4d^{9}> + \beta|3d^{9}4d^{10}\,L>$$

$$Ag^{III}\ d^{8}: |3d^{10}4d^{8}> \rightarrow \alpha|3d^{9}4d^{8}> + \beta|3d^{9}4d^{9}\,L> + \gamma|3d^{9}4d^{10}\,L^{2}>$$

[a] The initial ground states (left) are simplified as $|3d^{10}4d^{10-n}\rangle$ brackets.

metals. Surprisingly, these two XPS main contributions can be resolved notably better than the corresponding ones for AgO. If the shift in binding energy would be a measure of the extent of oxidation, the new phase $Ag_2Cu_2O_4$ should contain Ag more oxidized than Ag_2O, $Ag_2Cu_2O_3$, or even AgO, although stoichiometry counts would suggest the same overall oxidation state than in AgO.

There is also an alternative view. The electronic configuration of Ag^I can be represented by the bracket $|3d^{10}4d^{10}\rangle$, with a full closed 4d shell configuration. Photoionization of 3d electrons is expected to show only one component for each spin−orbit term and no multiplet splitting, as experimentally observed for $Ag_2Cu_2O_3$. On the other hand if silver is further oxidized, the 4d shell opens leading to multiple configurations and enabling multiple splitting for components other than d^{10} (See Scheme 1). Therefore, both the chemical shift and the appearance of multiplets are evidences of the qualitative oxidation of silver (the ≈1 eV energy shift between both lines in, e.g., Ag $3d_{5/2}$ of $Ag_2Cu_2O_4$, results from different contributions as core hole screening, Coulombic repulsion and charge transfer[40]). The extent in which that occurs is a different matter and would require configuration interaction calculations that are out of the scope of this paper.

Within this scenario, Ag 3d XPS for $Ag_2Cu_2O_4$ does not need to coincide necessarily with that of AgO, each spectrum depending on the particular combination of final state configurations (i.e., different α, β, and γ coefficients).

As compared to $Ag_2Cu_2O_4$, the ozone-treated samples (empty squares in Figure 3) and $AgCuO_2$ (full triangles in Figure 3) show higher XPS intensity for the lower binding energy feature. This is again ascribed to given combinations of final states that priorize higher oxidation states for silver. Therefore, $Ag_2Cu_2O_4$ (or $AgCuO_2$) exhibits oxidized silver but not necessarily *localized* mixed-valence states.

Silver oxidation states larger than +1 can also be inferred from the Auger Ag MVV lines (not shown). In this case the valley between Ag M_4VV and Ag M_5VV transitions is quite sensible to the degree of oxidation. For $Ag_2Cu_2O_3$ the valley is clearly deeper than that for AgO, $AgCuO_2$, or $Ag_2Cu_2O_4$.

On the other hand Cu 2p XPS signals remain identical after oxidation[12] as has been described before, with spectra resulting from satellite and multiple splitting, main peak $|p^5d^{10}L\rangle$ and satellite $|p^5d^9\rangle$, which allows multiple splitting because of the open shell nature. The apparent absence of change involves that the copper electronic configuration does not undergo a change upon oxidation of the precursor phase $Ag_2Cu_2O_3$.[9,14] However, XPS is not the most adequate technique to characterize higher oxidation states of Cu because of their low stability in UHV under irradiation.[9,14]

Remarkably, O 1s spectra also show interesting features. Upon oxidation, there is a significant shift to lower energies and broadening. Figure 4 shows the XPS spectra of the O 1s region for $Ag_2Cu_2O_3$ (empty diamonds in Figure 4) and $Ag_2Cu_2O_4$ obtained through various procedures (circles and triangles

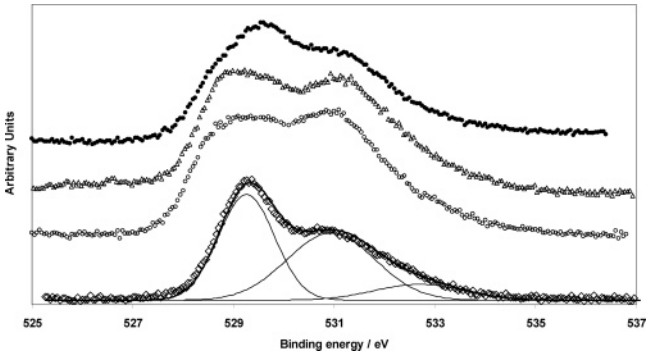

Figure 4. XPS spectra for the O 1s region for $Ag_2Cu_2O_3$ (◇), $Ag_2Cu_2O_4$ (electrochemical; ○), $Ag_2Cu_2O_{4.33}$ (oxidized with ozone; △), and $AgCuO_2$ (chemical $Ag_2Cu_2O_4$; ●).

in Figure 4) described in the text. The simplest least-squares fit (Gaussians) to the O 1s line of $Ag_2Cu_2O_3$ gives three components with binding energies of 529.3, 530.9, and 532.7 eV, respectively. The lower binding energy component is typical of transition metal oxides and corresponds in the first case to an Ag^I environment as, i.e., experimentally determined for Ag_2O.[35−38] Oxidized phases with the exception of AgO, however, show broader components splitted in two, with an overall shift toward lower energies. The observed downshift upon oxidation can be related to the participation of oxygen in the oxidation process and the corresponding increase in the covalence of the M−O bond.

The 530.9 and 532.7 eV components arise from dissolved/adsorbed (disordered) oxygen and hydroxides (probably at grain boundaries), respectively.[35,36,38] Note that for $Ag_2Cu_2O_4$ and $AgCuO_2$ the contribution of disorder becomes more evident than for $Ag_2Cu_2O_3$.[13]

The case of the O 1s signal for AgO (not shown) agrees with previous studies.[39] The metal−oxygen part corresponding to bonded oxygen is a single-component line despite the existence of both Ag^I and Ag^{III} and is slightly shifted toward lower binding energies and the disorder-induced part dominates over others giving an idea of the importance of disorder, or instability, in this material. Indeed the spectra of the electrochemically grown (empty circles in Figure 4), $Ag_2Cu_2O_4$ ozone-treated (empty triangles in Figure 4), and chemically synthesized $AgCuO_2$ (full circles Figure 4) samples are, as mentioned, noticeably much broader in the M−O component and can be tentatively resolved for the oxidized $Ag_2Cu_2O_4$ phases into two components at ≈528.7 and 529.6 eV, respectively. These values agree with reported measurements performed on AgO samples.[35,36] This ≈1 eV difference is in agreement with the splitting found also in Ag 3d lines and could be interpreted in terms of several types of M−O bonds or a considerable change in the electronic structure of oxygen. (As before, oxide ions, considered as an anion, O^{2-}, can be described as a full $2p^6$ shell, while oxidation would induce unpaired electrons and magnetism).

The changes in intensity for the signals typically assigned to disordered oxygen support the view of a phase that accommodates different degrees of disorder while still supporting the same basic structure. Oxygen disorder may come from ionic mobility (dynamic disorder), nonstoichiometry, or static mismatch and must be considered as an important aspect of this structure. Such disorder also involves unusual charge distributions and electron delocalization among the elements of the structure including possible mixed-valence states.

XPS data and structural refinements could be consistent if the oxidation of silver yields a mixed valence or intermediate state with a unique silver environment. That seems only possible

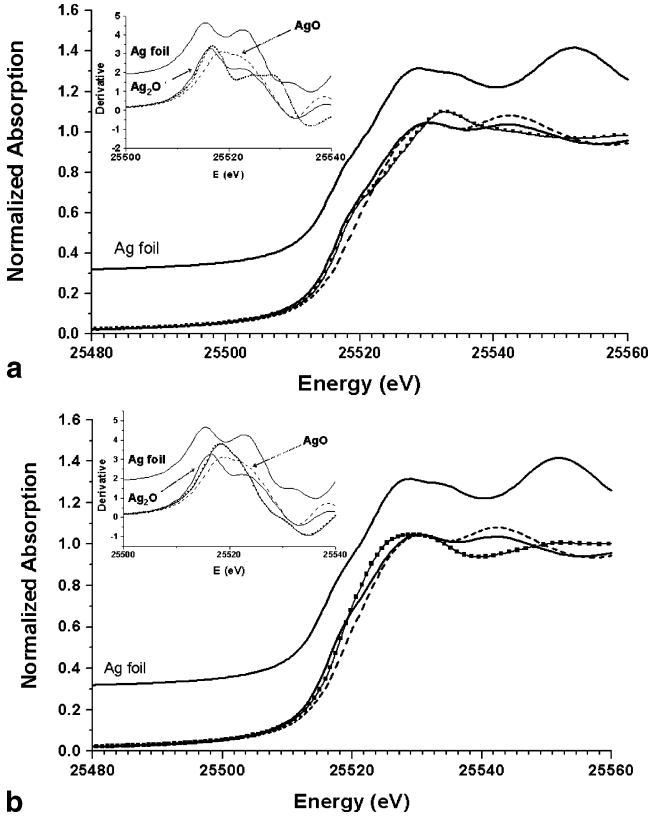

Figure 5. (a) Room-temperature normalized XANES spectrum at Ag K-edge for the $Ag_2Cu_2O_3$ sample compared to those of metallic silver and binary oxides. (Inset: first derivative of the normalized XANES spectra for (−) Ag_2O, (- -) AgO, and (-■-■-) $Ag_2Cu_2O_3$). (b) Room-temperature normalized XANES spectrum at Ag K-edge for the $Ag_2Cu_2O_4$ sample compared to those of metallic silver and binary oxides. (Inset: first derivative of the normalized XANES spectra for (−) Ag_2O, (- -) AgO, and (-■-■-) $Ag_2Cu_2O_4$).

with a mixed valence state classified as type II (fast hopping between $Ag^{I}-Ag^{III}$) or type III, total delocalization, in the Robin and Day classification scheme which would be equivalent to assign a Ag^{II} oxidation state.[41] In the first case, hopping of the electrons or holes between elements will be thermally activated with a slower exchange rate than the XPS time scale (10^{-16} s). In the second case the electronic description will be more similar to that of a metal, with no activation involved. The use of additional spectroscopic techniques as XANES and EXAFS and the temperature dependence of the signals are decisive to elucidate between both cases.

Both neutron diffraction at liquid helium and X-ray diffraction at liquid nitrogen have been performed and refined.[16] No dramatic change is observed upon cooling in the refinements other than the expected contraction of the atomic thermal ellipsoids, although remarkably the statistics are worst for low-temperature neutron data than for the high temperature.[16] No alternative structural model has been found.

XAS. XANES measurements for Ag and Cu K edges confirm for the bulk phase what XPS is showing for the surface. Figure 5 shows the XANES spectra at Ag, K edge, and Figure 6 at Cu, K edge, for both $Ag_2Cu_2O_3$ and $Ag_2Cu_2O_4$ and also a few reference phases.

In particular, the Ag K edge is related to the dipolar transition from deep 1s core levels to empty p states. The shape of the absorption edge is characterized by structures related with splittings of the 5p final states involving different 4d configurations. Therefore, those structures would have to be accounted for when the chemical shift of the absorption edge position, E_0, is

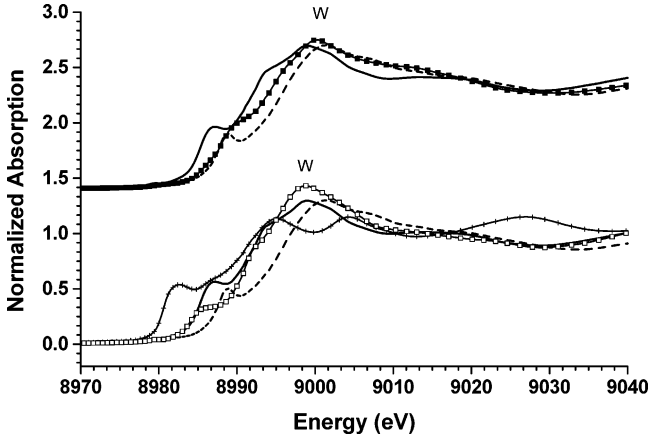

Figure 6. Room-temperature normalized XANES spectrum at Cu K-edge for the $Ag_2Cu_2O_3$ and $Ag_2Cu_2O_4$ samples compared to those of metallic copper and reference oxides ((-+) Cu foil; (−) CuO; (- -) $NaCuO_2$; (-□-□-) $Ag_2Cu_2O_3$; (-■-■-) $Ag_2Cu_2O_4$).

considered in order to evaluate oxidation states because it would only be linear for cases with similar local coordination geometry. With this in mind, Ag K edges are compared using the inflection point of the absorption edge determined by evaluating the maximum in their derivatives (see inset Figure 5).

Ag_2O and $Ag_2Cu_2O_3$, both presenting a shoulder before the absorption maximum, show the inflection point at 25517 eV (see Figure 5a) to be practically the same at any temperature, which involves the same oxidation state for both Ag^{I}. Both AgO and $Ag_2Cu_2O_4$ show a chemical shift to higher energies, at 25519.5 and 25518.6 eV respectively, without the presence of that shoulder (See Figure 5b). Since AgO is known to be oxidized, with a formal average oxidation state of +2, we must deduce that $Ag_2Cu_2O_4$ also presents oxidized silver, apparently to a smaller degree than the AgO, somewhere between +1 and +2 (+1.7 if the shift would be linearly correlated to the oxidation state).

XANES spectra at the Cu K absorption edge of $Ag_2Cu_2O_3$ and $Ag_2Cu_2O_4$ are shown in Figure 6 as compared with those of metallic copper and binary oxides. The general shape of the spectra presents more structure than that of silver, showing a main peak at the edge (labeled W in Figure 6). The main differences are related to the chemical shift. The energy positions of the absorption edge, measured as the maximum inflection point in the derivative spectrum (not shown), for CuO and $Ag_2Cu_2O_3$ are similar, 8992 and 8991 eV respectively, while those of $Ag_2Cu_2O_4$ and $NaCuO_2$ are also similar, 8994.5 and 8996 eV, respectively. The main conclusion from such comparison is that Cu in $Ag_2Cu_2O_4$ seems to be also more oxidized with respect to the state found in its precursor.

In summary, XANES experiments, which are sensitive to the bulk material, confirm the previous observations made by XPS on the existence of oxidized silver showing that we are not dealing just with a surface effect. The fact that XPS and XANES do not seem to show by linear interpolation the same extent of oxidation in the case of AgO and $Ag_2Cu_2O_4$ can be related to many factors, starting from a nonlinear dependence of the signal with oxidation state, to a more oxidized surface (or even to a change in charge distribution or coordination) depending on irradiation energy. But both types of techniques agree on the existence of oxidized silver near or above +2 oxidation state, and XANES shows that copper is also oxidized under these conditions and time scale.

From a different point of view, the analysis of the EXAFS spectra was done on the basis of previously reported crystal-

TABLE 2: Structural Summary of Distances (Å) and Angles (°) from X-ray Diffraction for Some Ag and Cu Oxides

bond (Å)	$Ag_2Cu_2O_3$[3,4]	$Ag_2Cu_2O_4$[13]	Ag_2O[42]	AgO[26]	CuO[43]	$NaCuO_2$[44]
Ag−O	2 × 2.073	2 × 2.254	2 × 2.061	2 × 2.1466 (I)		
	4 × 3.480	4 × 2.742	6 × 3.912	2 × 2.0084 (III)		
				2 × 2.0358 (III)		
Cu−O	2 × 1.906	4 × 1.827			2 × 1.955	4 × 1.839, 2 × 3.046
	2 × 1.988	2 × 2.703			2 × 1.957	
Cu−Cu	2 × 2.943	2 × 2.800			4 × 2.900	2 × 2.753
	4 × 3.387	4 × 3.335			4 × 3.082	4 × 3.467
Ag−Ag	2 × 2.9431	2 × 2.800	3.366	3.244 (I−I) (III−III)		
	4 × 3.3871	4 × 3.335	4.760	3.401 (I−III)		
Cu−Ag	2 × 2.943	4 × 3.243				
	4 × 3.387	2 × 3.503				
O−O	2 × 2.47	2 × 2.348	4.1223	2 × 2.823	2 × 2.626	1 × 2.459
	4 × 2.94	2 × 2.800		2 × 2.896	2 × 2.896	2 × 2.753

angle (°)	$Ag_2Cu_2O_3$	$Ag_2Cu_2O_4$	Ag_2O	AgO	CuO	$NaCuO_2$
O−Ag−O	180	180	180	84.547		
				91.454		
O−Cu−O	79.9	79.7			84.31	2 × 180
	100.1	100			95.69	2 × 96.45
						2 × 83.55
Cu−O−Ag	116.61	104.8				
Cu−O−Cu	104.7	90			84.31	96.45
	116.865				95.37	
					103.97	
Ag−O−Ag	90.44		109.471	106.671		
			58.518	106.335 (I−O−III)		
				109.827 (I−O−III)		

lographic refinements for these phases. Those are represented in Table 2. In first place, copper coordination is square-planar in both silver cuprates, with four Cu−O distances that become shorter upon oxidation, 1.91 and 1.99 Å in $Ag_2Cu_2O_3$ to 1.83 Å in $Ag_2Cu_2O_4$. On the other hand, O−O distances are shorter than in any other silver or copper oxide.

With respect to silver, the two shorter Ag−O distances in the oxidized phase $Ag_2Cu_2O_4$, are larger than those found in the linear coordination cases Ag_2O, AgO, or $Ag_2Cu_2O_3$, even though oxidation should imply a shortening of the Ag−O linear bonds for the same coordination number. In fact, $Ag_2Cu_2O_4$ presents two short Ag−O distances, 2.2 Å, longer than the 2.07 Å from $Ag_2Cu_2O_3$ (linear Ag^I) or the 2.06 Å from Ag_2O and 2.01 and 2.14 Å from AgO (Ag^{III} and Ag^I respectively). The second set of Ag−O distances for $Ag_2Cu_2O_4$ are at 2.74 Å, much shorter than the 3.48 and 3.91 Å, from $Ag_2Cu_2O_3$ and Ag_2O. The increase in the shortest distance upon oxidation can only be understood simultaneously to the shortening of the next four Ag−O distances, much shorter than usual, that can equilibrate the actual charge on the ion raising the coordination number toward six. Some time ago, hybridization of s and d_{z^2} orbitals in both metals were used to explain the linear covalent bonds in the case of Cu^I and Ag^I [45] which allow oxygen to be closer than expected from the sum of ionic radii. But also, examples of octahedral (2 + 4) Ag^IO_6 have been described,[46] assuming +1 oxidation states. However, in relative terms, the increase in Ag−O shortest distances upon oxidation is correlated with an increase in coordination number, since the next four longer Ag−O distances get shorter. Estimations based on the bond valence approach[16] fully agree with this perspective. We are therefore observing a distorted octahedral environment for oxidized silver, which could be described formally as $Ag^{II}O_6$.

It must be taken into account, however, that long-range disorder can show up as an increase in coordination number. Therefore, it is important to complement crystallographic evidence with information from local structure extracted from the EXAFS analysis.

Figure 7 shows the Cu K-edge EXAFS spectra and the modulus of the Fourier transform at room temperature for CuO, $NaCuO_2$, $Ag_2Cu_2O_3$, and $Ag_2Cu_2O_4$. EXAFS spectra of $Ag_2Cu_2O_3$ and CuO present similar structures while the one for $Ag_2Cu_2O_4$, is much more similar to that of $NaCuO_2$. The Fourier

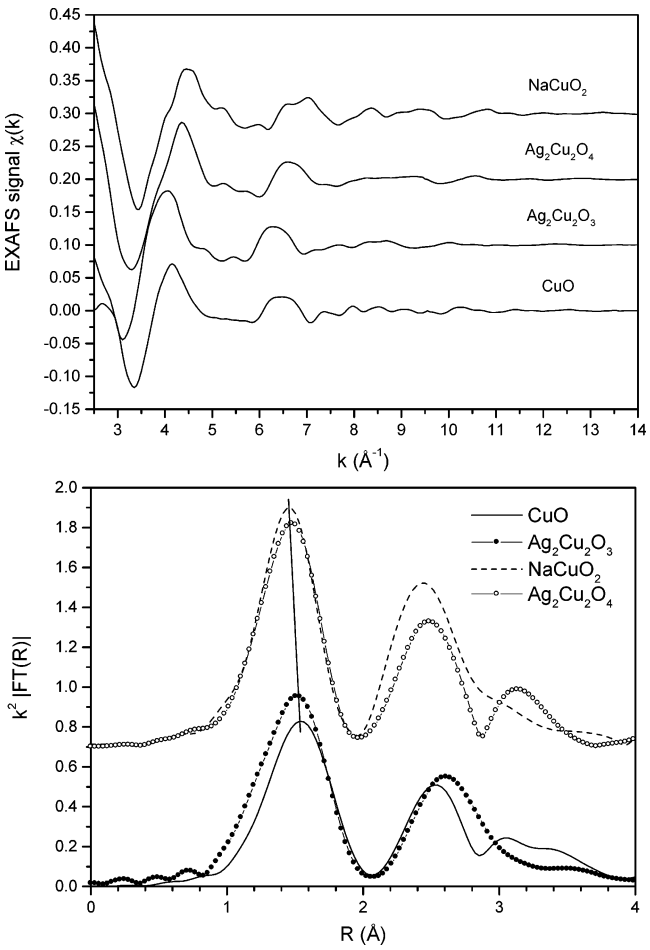

Figure 7. Top: EXAFS spectra at the Cu K-edge of $Ag_2Cu_2O_3$ and $Ag_2Cu_2O_4$ samples compared to those of reference oxides at room temperature. Bottom: Fourier transform of the experimental $k^2\chi(k)$ signals for these samples.

TABLE 3: Best-Fit Results from the Structural Analysis of the First Coordination Shell at Cu K-edge of $Ag_2Cu_2O_3$ and $Ag_2Cu_2O_4$ Samples Compared to CuO and $NaCuO_2$ Reference Oxides at Room Temperature[a]

		CuO		$Ag_2Cu_2O_3$		$NaCuO_2$		$Ag_2Cu_2O_4$	
path	*N*	*R* (Å)	σ^2 (Å^2)	*R* (Å)	σ^2 (Å^2)	*R* (Å)	σ^2 (Å^2)	*R* (Å)	σ^2 (Å^2)
Cu−O	4	1.953(4)	0.0040(3)	1.949(2)[b]	0.0047(2)	1.850(4)	0.0040(3)	1.885(2)	0.0041(2)
	2	2.748(30)	0.0054(9)					2.799(50)	0.022(10)

[a] *N* is the coordination number (fixed), *R* is the interatomic distance, and σ^2 is the Debye−Waller factor (the overall factor S_0^2 was fixed to 0.85). Numbers in parentheses are statistical errors in the last significant digit. [b] A distortion ($2 \times 1.910(3)/2 \times 1.987(3)$) with smaller $\sigma^2 = 0.0031(4)$ Å^2 gives the same goodness of the fit.

TABLE 4: Best-Fit Results from the Structural Analysis of the Second Coordination Shell at the Cu K-edge of $Ag_2Cu_2O_3$ and $Ag_2Cu_2O_4$ Samples Compared to CuO and $NaCuO_2$ Reference Oxides at Room Temperature[a]

	N	*R* (Å)	σ^2 (10^{-3} Å^2)
		CuO	
Cu−Cu	4	2.90(1)	0.0054(9)
	4	3.06(2)	0.010(2)
	2	3.15(2)	0.010(2)
	2	3.45(3)	0.009(4)
	2	3.78(6)	0.011(7)
		$Ag_2Cu_2O_3$	
Cu−Cu	2	2.945(8)	0.005(2)
	4	3.421(40)	0.006(2)
Cu−Ag	2	2.945(8)	0.013(9)
	4	3.421(40)	0.007(2)
		$NaCuO_2$	
Cu−Cu	2	2.764(4)	0.0030(3)
	4	3.502(15)	0.016(2)
		$Ag_2Cu_2O_4$	
Cu−Cu	2	2.827(4)	0.0050(4)
	4	3.391(20)	0.019(4)
Cu−Ag	4	3.270(2)	0.014(2)
	2	3.530(2)	0.014(2)

[a] *N* is the coordination number (fixed), *R* is the interatomic distance, and σ^2 is the Debye−Waller factor in each case (the overall factor S_0^2 was fixed to 0.85). Numbers in parentheses are statistical errors in the last significant digit.

transform (FT) of the κ^2-weighted EXAFS spectra was calculated between 2.2 and 14 Å^{-1} using a Gaussian window. We observe a main peak, between 1 and 2 Å ascribed to the first oxygen shell and further peaks that correspond to successive coordination shells. The position of the FT first peak shifts toward lower values for both $NaCuO_2$ and $Ag_2Cu_2O_4$ indicating a decrease in the Cu−O distance. The main results of the structural analysis at Cu K-edge are summarized in Tables 3 and 4 for the first and second coordination shells, respectively, and Figure 8 presents the best-fit simulations. The structural parameters resulted in good agreement with the crystallographic data (see Tables 2 and 3). A square planar environment is observed for both $Ag_2Cu_2O_3$ and $Ag_2Cu_2O_4$. We observe a decrease of the Cu−O distance from about 1.95 Å in CuO and $Ag_2Cu_2O_3$ to 1.885 Å in $Ag_2Cu_2O_4$ and 1.850 Å in $NaCuO_2$ respectively. This decrease agrees with the chemical shift observed in XANES spectra and it is consistent with an increase in copper oxidation state upon oxidation. It is noteworthy that $Ag_2Cu_2O_3$ has a higher Debye−Waller factor for the first copper coordination shell. Since this factor is also related to the spread of Cu−O distances, it implies the presence of some kind of distortion around the Cu atom. Moreover, two short (1.91 Å) and two long (1.99 Å) distances with lower Debye−Waller factors give the same goodness of fit. There is not substantial temperature dependence. In general, interatomic distances will shorten due to thermal contraction and Debye−Waller factors decreased due to smaller thermal motion.

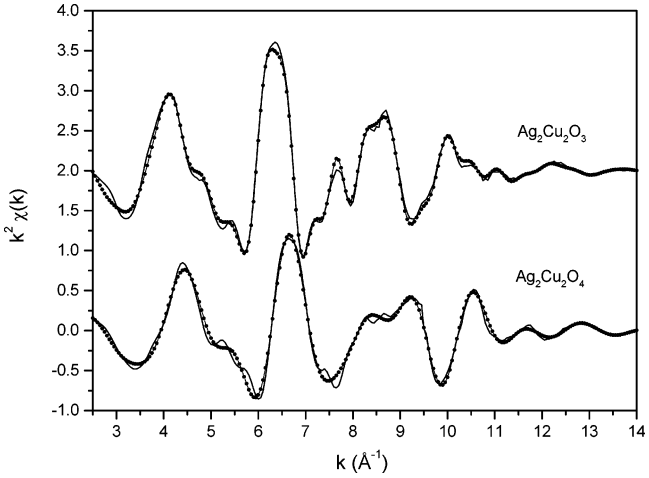

Figure 8. $k^2\chi(k)$ EXAFS spectra (solid line) at the Cu K-edge of $Ag_2Cu_2O_3$ and $Ag_2Cu_2O_4$ samples compared to the best-fit (line + dots) at room temperature.

TABLE 5: Best-Fit Results from the Structural Analysis of the First Coordination Shell (Ag−O Bonds) at the Ag K-edge of $Ag_2Cu_2O_3$ and $Ag_2Cu_2O_4$ Samples Compared to Ag_2O and AgO Reference Oxides as a Function of Temperature[a]

sample	*T* (K)	N	R_{Cris} (Å)	R_{EXAFS} (Å)	σ^2 (10^{-3} Å^2)
		Ag K Edge Data			
Ag_2O	300	2	2.044	2.07 ± 0.005	3.2 ± 0.7
(Ag^I- linear)	30	2		2.06 ± 0.004	2.4 ± 0.4
$Ag_2Cu_2O_3$	300	2	2.13	2.08 ± 0.004	2.6 ± 0.3
(Ag^I- linear)	180	2		2.08 ± 0.004	2.1 ± 0.3
	90	2		2.07 ± 0.004	1.8 ± 0.3
	40	2		2.07 ± 0.005	1.8 ± 0.4
AgO	300	2	2.16	2.13 ± 0.02	4.6 ± 3
($Ag^I + Ag^{III}$)		4	2.80		
		4	2.025	2.01 ± 0.01	3 ± 1
		2	2.81	2.79 ± 0.03	20 ± 5
	40	2		2.13 ± 0.02	3.8 ± 4
		4			
		4		2.01 ± 0.01	2.5 ± 1
		2		2.76 ± 0.03	10 ± 4
$Ag_2Cu_2O_4$	300	2	2.252	2.20 ± 0.01	8 ± 0.5
($Ag^{+1.7}$)		4	2.741	2.70 ± 0.04	19 ± 2
	180	2		2.18 ± 0.01	6 ± 0.7
		4		2.69 ± 0.03	13 ± 2
	90	2		2.19 ± 0.01	4 ± 0.6
		4		2.71 ± 0.02	10 ± 2
	30	2		2.19 ± 0.01	4 ± 0.7
		4		2.70 ± 0.02	8 ± 2

[a] *N*: coordination number (fixed). R_{Cris}: crystallographic interatomic distances. R_{EXAFS}: EXAFS refined interatomic distances. σ^2: Debye−Waller factor. The overall reduction factor S_0^2 was fixed to 0.83, obtained for Ag_2O.

On the other hand EXAFS data are rather peculiar for Ag. Figure 9 shows the EXAFS spectra and the modulus of the κ^2-weighted FT at the Ag K-edge taken between 2.5 and 16 Å^{-1} at 30 K. The first peak (first Ag−O coordination shell) is alike

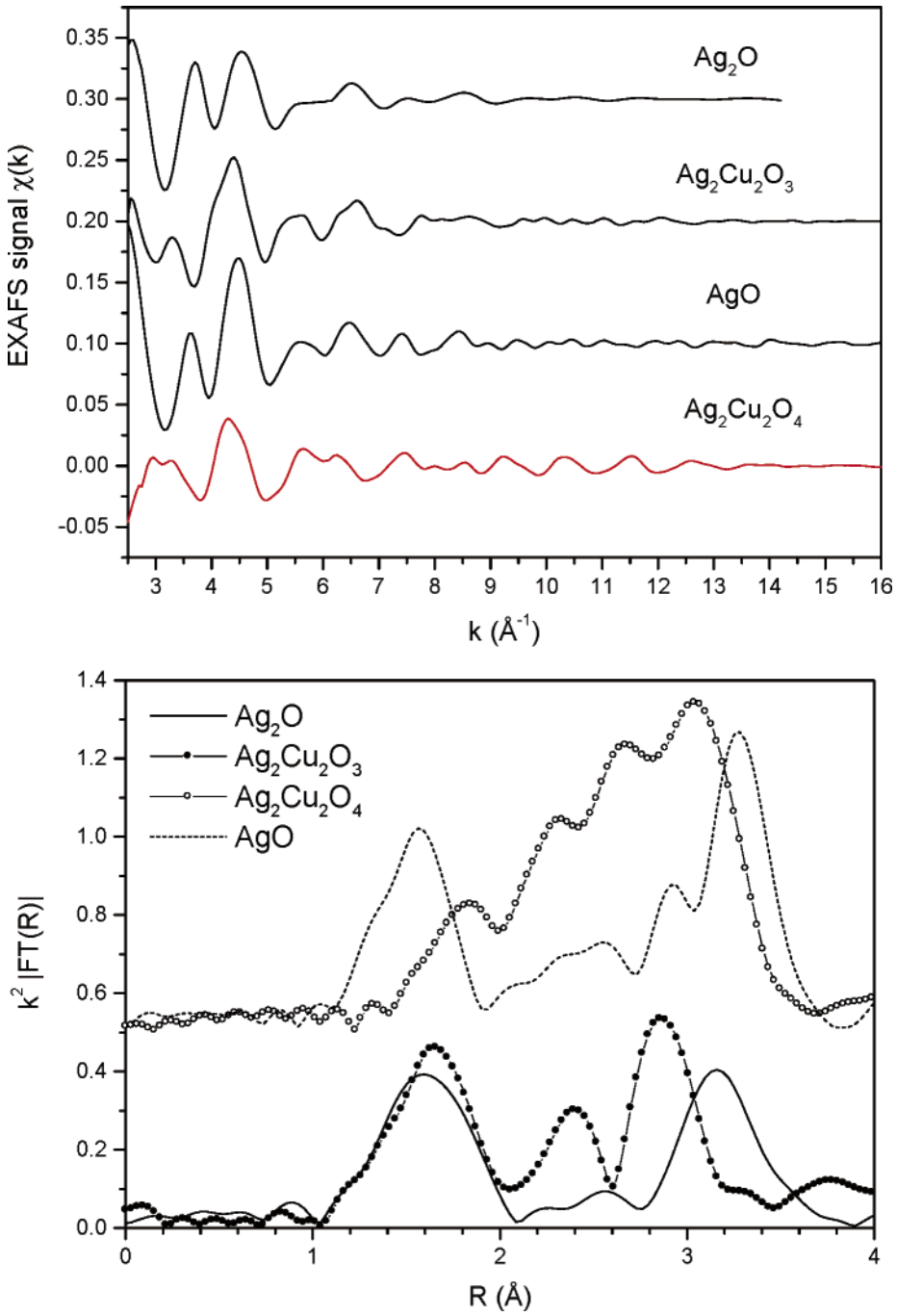

Figure 9. Top: EXAFS spectra at the Ag K-edge of $Ag_2Cu_2O_3$ and $Ag_2Cu_2O_4$ samples compared to those of reference oxides at $T = 30$ K. Bottom: Fourier transform of the experimental $k^2\chi(k)$ signals for these samples.

for Ag_2O and $Ag_2Cu_2O_3$ as expected from the linear coordinated Ag^I in both cases. A slight shift to lower values in the peak position is observed for AgO according to the higher oxidation state of silver in this compound. However, the position of this first peak in $Ag_2Cu_2O_4$ involves an increase in distances which could appear to contradict the oxidation of silver that both XANES and XPS experiments show, but that is absolutely consistent with diffraction data.

The structural analysis at the Ag K-edge is summarized in Tables 5 and 6. Best fits obtained at $T = 30$ K at the Ag K-edge for $Ag_2Cu_2O_3$ and $Ag_2Cu_2O_4$ are illustrated in Figure 10. First and second coordination shells have been included in the fit. Very similar refinements are obtained for $Ag_2Cu_2O_3$ and Ag_2O that agree with a linear coordination and a Ag−O distance of 2.08 Å as expected for Ag^I. The Debye−Waller factor for the Ag−O distance in $Ag_2Cu_2O_3$ follows the standard evolution with temperature for a regular environment, becoming lower as the temperature is lowered and the phonons vibration decreases. This behavior is clearly seen in Figure 11 where the peak at 1.7 Å increases upon cooling equally for both phases, $Ag_2Cu_2O_3$ and Ag_2O.

AgO presents two types of environments for silver, linear and square-planar, and both are necessary in order to fit the Ag K-edge EXAFS data (see Table 2 and 5). It has been assumed from crystallography that these two environments for Ag in AgO would correspond to two different oxidation states, Ag^I and Ag^{III} respectively, and it is logical to assume here the same. On the contrary, $Ag_2Cu_2O_4$ fits well only when using a single type of silver environment exactly as in the crystallography refinement, at any temperature, with Ag−O distances refined being con-

TABLE 6: Best-Fit Results from the Structural Analysis of the Second Coordination Shell (Ag−O Bonds) at the Ag K-edge of $Ag_2Cu_2O_3$ and $Ag_2Cu_2O_4$ Samples Compared to Ag_2O and AgO Reference Oxides as a Function of Temperature[a]

sample	T (K)	N	Ag−Ag (Å) R_{Cris}	Ag−Ag (Å) R_{EXAFS}	σ^2 (10^{-3} Å^2)	N	Ag−Cu (Å) R_{Cris}	Ag−Cu (Å) R_{EXAFS}	σ^2 (10^{-3} Å^2)
				Ag K Edge Data					
Ag_2O	300	12	3.337	3.34 ± 0.04	51 ± 9				
(Ag^I linear)	30	12		3.33 ± 0.01	16 ± 0.4				
$Ag_2Cu_2O_3$	300	2	2.943	2.93 ± 0.01	9 ± 2	2	2.943	2.95 ± 0.01	10 ± 2
(Ag^I linear)		4	3.386	3.51 ± 0.08	30 ± 10	4	3.386	3.42 ± 0.02	10 ± 2
	180	2		2.93 ± 0.01	7 ± 1	2		2.95 ± 0.01	8 ± 2
		4		3.24 ± 0.1	40 ± 30	4		3.40 ± 0.02	7 ± 3
	90	2		2.93 ± 0.01	4 ± 1	2		2.94 ± 0.01	4 ± 1
		4		3.37 ± 0.03	20 ± 5	4		3.40 ± 0.01	4 ± 0.5
	40	2		2.94 ± 0.01	3 ± 1	2		2.94 ± 0.01	4 ± 2
		4		3.39 ± 0.02	5 ± 4	4		3.39 ± 0.02	2 ± 2
AgO	300	6	3.291	3.28 ± 0.01	7 ± 0.5				
(Ag^I linear		6	3.433	3.44 ± 0.01	9 ± 1				
$+Ag^{III}$ planar)									
	40	6		3.28 ± 0.005	3 ± 0.5				
		6		3.43 ± 0.01	2 ± 1				
$Ag_2Cu_2O_4$	300	2	2.800	2.79 ± 0.01	9 ± 1	4	3.243	3.27 ± 0.01	13 ± 1
($Ag^{+1.5} \approx$ linear)		4	3.335	3.43 ± 0.04	30 ± 5	2	3.503	3.53 ± 0.01	13 ± 1
	180	2		2.80 ± 0.01	6 ± 1	4		3.27 ± 0.01	11 ± 3
		4		3.36 ± 0.03	10 ± 2	2		3.54 ± 0.01	11 ± 3
	90	2		2.81 ± 0.005	4 ± 0.5	4		3.28 ± 0.01	8 ± 2
		4		3.35 ± 0.01	6 ± 1	2		3.54 ± 0.01	8 ± 2
	30	2		2.81 ± 0.005	3 ± 0.5	4		3.27 ± 0.01	6 ± 1
		4		3.34 ± 0.01	5 ± 1	2		3.53 ± 0.01	6 ± 1

[a] N: coordination number (fixed). R_{Cris}: crystallographic interatomic distances. R_{EXAFS}: EXAFS refined interatomic distances. σ^2: Debye−Waller factor. The overall reduction factor S_0^2 was fixed to 0.83, obtained for Ag_2O.

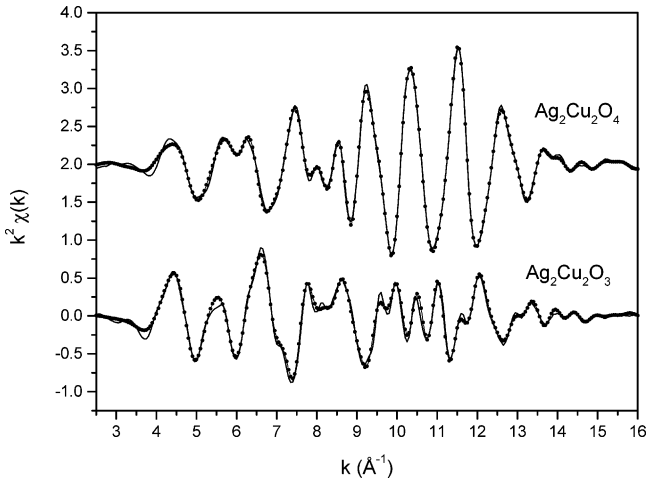

Figure 10. Best-fit at $T = 30$ K for $Ag_2Cu_2O_4$ and $Ag_2Cu_2O_3$ at Ag K-edge of $k^2\chi(k)$ signals, similar to Cu K-edge.

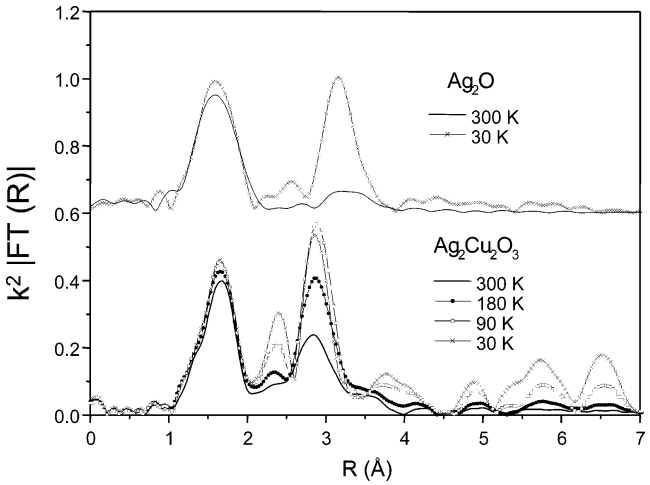

Figure 11. Fourier transform of the $k^2\chi(k)$ EXAFS spectra of $Ag_2Cu_2O_3$ and Ag_2O taken at fixed temperatures between 30 K and room temperature.

sistent also with those obtained from X-ray diffraction data. It has not been possible to find an alternative refinement with two types of environments for silver. On the other hand, the environment observed seems linear at first sight, but the distances are also longer than expected when an oxidation occurs, 2.20 Å (vs 2.08). The second set of Ag−O distances correspond to four atoms of oxygen at only 2.74 Å which is a distance very similar to the next set of silver atoms at a distance of 2.79 Å. All those data agree in a significant manner with long range, large time scale, diffraction data. Temperature dependence of the EXAFS data (Figure 12) and the corresponding refinements (Tables 5 and 6) show a clear continuous change, with an increased ordering as the oxide is cooled. The change is gradual and does not show any phase transition or sharp turning point.

Therefore, the same effect is observed in this local structure (short-time scale) probe than in the crystallographic discussion based on long time scale, space averaged diffraction data: A coordination change seems to be occurring upon oxidation and the linear description is no longer valid since the Ag−O short distances increase and four new distances appear to be too short to avoid accounting for them. (Actually bond valence calculations require their use to fulfill the silver charge whatever the B_0 parameters chosen.) The surprising contribution of the second set of Ag−O distances 4×2.70 Å, so similar to the first Ag−Ag distances, appears in both crystallographic and spectroscopic measurements, which makes the results internally consistent, and describe silver, as Ag^{II} (or near +2) in a deformated octahedral environment, excluding a possible thermally activated hoping slower than time scales of XPS or XAS.

Those unusual structural features may be at the center of the structure flexibility, disorder or meta-stability, and get this phase closer to previously reported silver fluorides[7,8,47] since they suggest the existence of oxidized silver with formal oxidation states near +2 in an oxide near octahedral environment.

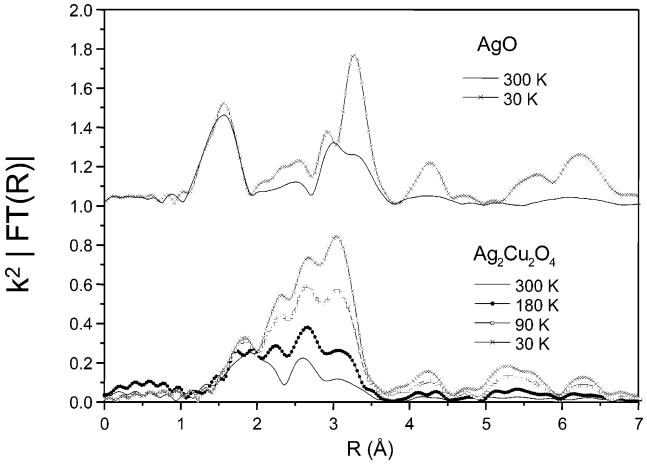

Figure 12. Fourier Transform of the $k^2\chi(k)$ EXAFS spectra of $Ag_2Cu_2O_2$ and AgO taken at fixed temperatures between 30 K and room temperature.

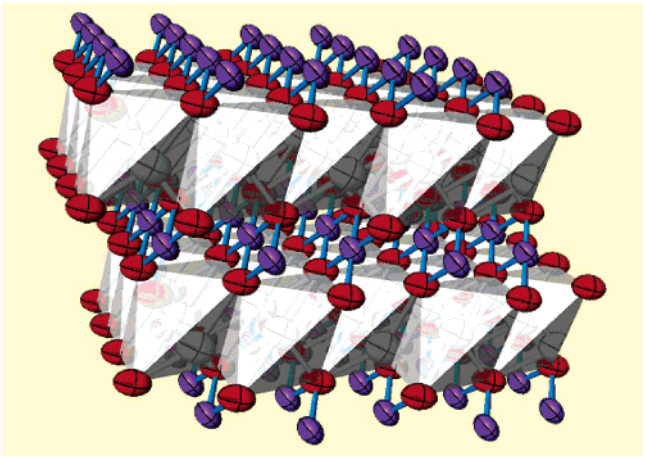

Figure 13. Alternative description of $Ag_2Cu_2O_4$ with octahedral Ag−O_6 (2 + 4), showing in second term inner coordination.

Furthermore, Ag^{II} has been reported to present weak paramagnetism in many cases,[47] just as has been reported before for this case.[12,16]

Curiously enough, when moving to the second coordination sphere, Ag−Ag distances rather short, the Debye−Waller factors for the second sphere are not so large and seem to have accommodated the possible distortions in the structure.

Therefore, and although AgO was originally taken as a structural and electronic model for the new phase $Ag_2Cu_2O_4$, it is only partially an appropriate model and may be should not be taken as a unique reference in the future. $Ag_2Cu_2O_4$ is presenting oxidized silver and copper, and it is highly probable that oxygen also participates in this oxidation scheme, according to the observations made by XPS, and the phase may become a new reference point based on those electronic features. No valence splitting can be assigned in $Ag_2Cu_2O_4$ to different silver atoms, but rather a mixed valence delocalized system with a single type of silver environment is observed at any time scale, with any technique and at any temperature. If that could yield long-range properties it would be expected to be metallic. In that single type of environment silver is better described as coordinated in a distorted octahedron with two axial short bonds at 2.2 Å and four equatorial Ag−O bonds at 2.80 Å that cannot be neglected and contribute to the charge and to the actual description of the bonding. Figure 13 represents the structure based on this new description. Ag−Ag distances are very similar to the second Ag−O distances and involve a peculiar description for M−M and M−O bonds in the structure. Theoretical calculations become mandatory in order to elucidate the electronic structure of this material. It is also clear that the phase seems to present some degree of disorder and/or ion mobility for each element hard to quantify. It is highly probable that such flexibility is also at the heart of its stability.

Conclusions

The integration of structural and spectroscopic local structure parameters for $Ag_2Cu_2O_4$ and their comparison with those of $Ag_2Cu_2O_3$, AgO, Ag_2O, $NaCuO_2$, and CuO shows that oxidation occurs in all elements of the phase and that a variable charge distribution and delocalization within the structure is possible depending on the synthesis procedure, irradiation, and extent of oxidation. Although AgO was originally taken as a structural and electronic model for the new phase $Ag_2Cu_2O_4$, it is only partially an appropriate model and may be should not be taken as a unique reference in the future. $Ag_2Cu_2O_4$ is presenting oxidized silver and copper, and oxygen also participates in this oxidation scheme, according to the observations made by XPS. The phase may be becoming itself a new reference. No valence splitting or disproportionation can be found for silver in $Ag_2Cu_2O_4$, but rather a delocalized system with a single type of silver environment is observed at any time scale, with any technique and at any temperature that involves a large extent of charge delocalization among atoms in a metal-like behavior. In that single type of environment silver coordination is better described as a rather tetragonally elongated octahedron with two axial short bonds at 2.2 Å and four equatorial Ag−O bonds at 2.80 Å that cannot be neglected and contribute to the charge and to the actual description of the bonding. It would seem again as if the structure could accommodate some changes in the charge distribution and disorder without breaking the main structural features, in a fashion similar to the behavior of AgI above 150 °C where literally the "silver framework melts" within the iodide crystalline ordering.[48]

While is not the first case where Ag coordination can be described as octahedral (2+4), the comparison of distances among phases with different oxidation states shows the large flexibility that silver can present in its coordination to adjust valence changes. Copper also shows evidence, from crystallographic and spectroscopic data, of being oxidized and sharing the charge distribution with both silver and oxygen. The combination of both metals enhance the possibility of charge delocalization while possible ionic mobility and disorder may be underlying the phenomena observed in this structure that seems to show a peculiar flexibility and would recommend a further configuration interaction study.

Acknowledgment. We are thankful for financing from the Spanish Ministry of Science and Education (PB-98-0491, MAT 2002-04529) and for a graduate fellowship for D.M.R.. Thanks are also due for a prize from the Fundacion Domingo Martínez. We also acknowledge R. I. Walton and J. Garcia for comments and corrections. Dedicated to Prof. Jansen on his 60th birthday.

References and Notes

(1) (a) Baker, C. L.; Lincoln, F. J.; Johnson, A. W. S. *Acta Crystallogr. B* **1991**, *104*, 891. (b) Baker, C. L.; Lincoln, F. J.; Johnson, A. W. S. *Aust. J. Chem.* **1992**, *45*, 1441. (c) Frueh, A. J.; Czamanske, G. K.; Knight, C. Z. *Kristallogr., Kristallgeom.* **1957**, *108*, 389. (d) Avilov, A. S.; Baranova, R. V. *Kristallografiya* **1972**, *17*, 219.

(2) Tejada-Rosales, E. M.; Palacín M. R.; Gómez-Romero, P. *Bol. Soc. Esp. Cerám. Vidrio* **2000**, *39* (3), 209.

(3) Gómez-Romero, P.; Tejada-Rosales, E. M.; Palacín, M. R. *Angew. Chem. Int. Ed.* **1999**, *38* (4), 524.
(4) Tejada-Rosales, E. M.; Rodríguez-Carvajal, J.; Casañ-Pastor, N.; Alemany, P.; Ruiz, E.; Alvarez, S.; Gómez-Romero, P. *Inorg. Chem.* **2002**, *41*, 6604.
(5) Tejada-Rosales, E. M.; Oró-Solé, J.; Gómez-Romero, P. **2002**, *163* (1), 151.
(6) McMillan, J. A. *Chem. Rev.* **1962**, *62*, 65.
(7) Ebert, M. S.; Rodowskas, E. L.; Frazer, J. C. W. *J. Am. Chem. Soc.* **1933**, *55*, 3056.
(8) (a) Grochala, W.; Hoffman, R. *Angew. Chem., Int. Ed.* **2001**, *40*, 2742. (b) Grochala, W.; Egdell, R. G.; Edwards, P. P.; Mazej, Z.; Zemva, B. *Chem. Phys. Chem.* **2003**, *4*, 997.
(9) Vanderah, T. A. *Chemistry of Superconductor Materials. Preparation, Chemistry, Characterization and Theory*; Noyes Publications: Mill Road, 1992.
(10) Casañ-Pastor, N.; Gómez-Romero, P.; Fuertes, A.; Navarro, J. M.; Sanchis, J. M.; Ordoño-Castillo, S *Physica C* **1993**, *216*, 478.
(11) Muñoz-Rojas, D.; Tejada-Rosales, E. M.; Gómez-Romero, P.; Casañ Pastor, N. Poster and oral presentations at Vth Electroceramics and FIGIPS Meeting in Barcelona, May-June 2001.
(12) Muñoz-Rojas, D.; Oró, J.; Gómez-Romero, P.; Fraxedas, J.; Casañ-Pastor, N. *Electrochem. Commun.* **2002**, *4*, 684.
(13) Muñoz-Rojas, D.; Fraxedas, J.; Oró, J.; Gómez-Romero, P.; Casañ-Pastor, N. *Cryst. Eng.* **2002**, *5*, 459.
(14) Muñoz-Rojas, D.; Fraxedas, J.; Gómez-Romero, P.; Casañ-Pastor, N. *J. Solid State Chem.* **2005**, *178*, 295.
(15) Curda, J.; Klein, W.; Liu, H.; Jansen, M. *J. Alloys Compd.* **2002**, *338*, 99.
(16) Muñoz-Rojas, D. New Ag−Cu Oxides by Electrochemical Intercalation and other soft methods. Ph.D. Thesis, Autonomous University of Barcelona (UAB), May 2004.
(17) Wattiaux, A.; Park, J. C.; Grenier, J. C.; Pouchard, M. *C. R. Acad. Sci. Paris Serie II* **1990**, *310*, 1047.
(18) Ordoño-Castillo, S.; Michel, C. R.; Seffar, A.; Fontcuberta, F.; Casañ-Pastor, N. *Physica C* **1994**, *235*−*240*, 563.
(19) Michel, C. M.; Casañ-Pastor, N. *Physica C* **1997**, *278*, 149.
(20) Casañ-Pastor, N.; Michel, C. R.; Zinck, C.; Tejada-Rosales, E. M. *Chem. Mater.* **2001**, *13*, 2118.
(21) Grenier, J. C.; Wattiaux, A.; Lagueyte, N.; Park, J. C.; Marquestaut, E.; Etorneau, J.; Pouchard, M. *Physica C* **1991**, *173*, 139.
(22) Gómez-Romero, P.; Palacín, M. R.; Michel, C. R.; Casañ-Pastor, N. *Solid State Ion.* **1997**, *101*−*103*, 411.
(23) Michel, C. R.; Amigó, R.; Casañ-Pastor, N. *Chem. Mater.* **1999**, *11*, 195.
(24) Tejada-Rosales, E. M. Complex Oxides of Silver and Copper. Ph.D. Thesis, Autonomous University of Barcelona (UAB), Jan. 2001.
(25) Adelsberger, K.; Curda, J.; Vensky, S.; Jansen, M. *J. Solid State Chem.* **2001**, *158*(1), 82.
(26) Jansen, M.; Fischer, P. *J. Less-Common Met.* **1988**, *137* (1−2), 123.
(27) Choy, J. H.; Kim, Y. I.; Hwang, S. J. *J. Phys. Chem.* **1998**, *102*, 9191.
(28) Behrens, P.; Assmann, S.; Bilow, U.; Linke, C.; Jansen, M. *Z. Anorg. Allg. Chem.* **1999**, *625*, 111.
(29) Allen, P. G.; Gash, A. E.; Dorhout, P. K.; Strauss, S. H. *Chem. Mater.* **2001**, *13*, 2257.
(30) Curda, J.; klein, W.; Jansen, M. *J. Solid State Chem.* **2001**, *162*, 220.
(31) Friedman, T. L.; Stacy, A. M. *J. Solid State Chem.* **1994**, *109*, 203.
(32) Filiponi, A.; Borowski, M.; Bowron, D. T.; Ansell, S.; A. Di Cicco, A.; de Panfilis, S.; Itiè, J. P. *Rev. Sci. Instrum.* **2002**, *71*, 2422.
(33) Koningsberger, D. C.; Prins, R. *X-Ray absorption: Principles, Application, Techniques of EXAFS, SEXAFS and XANES*; Wiley: New York, 1988.
(34) (a) Rehr, J. J.; Albers, R. C. *Rev. Mod. Phys.* **2002**, *72*, 621. See http://FEFF.phys.washington.edu. (b) Stern, E. A.; Newville, H.; Ravel, B.; Yaroby, Y.; Haskel, D. *Physica B* **1995**, *208&209*, 117.
(35) Schön, G. *Acta Chem. Scand.* **1973**, *27*, 24623.
(36) Bao, X.; Muhler, M.; Schedel-Niedrig, T.; Schlögl, R. *Phys. Rev. B* **1996**, *54*, 2249.
(37) Tjeng, L. H.; Meinders, M. B. J.; van Elp, J.; Ghijsen, J.; Sawatzky, G. A.; Johnson, R. L. *Phys. Rev. B* **1990**, *41*, 3190.
(38) Waterhouse, G. I. N.; Bowmaker, G. A.; Metson, J. B. *Appl. Surf. Sci.* **2001**, *183*, 191.
(39) Boronin, A. I.; Koscheev, S. V.; Zhidomirov, O. V. K. G. M. *React. Kinet. Catal. Lett.* **1998**, *63*, 291.
(40) Ghijsen, J.; Tjeng, L. H.; van Elp, J.; Eskes, H.; Westerink, J.; Sawaztzky, G. A.; Czyzyk, M. T. *Phys. Rev. B.* **1998**, *38*, 11332.
(41) Cox, P. A. *The Electronic Structure and Chemistry of Solids*; Oxford Science Publications: Walton Street, Oxford OX26DP, U.K., 1989.
(42) Norby, P.; Dinnebier, R. E.; Fitch, A. N. *Inorg. Chem.* **2002**, *41*, 3628.
(43) Brese, N. E.; O'Keefe, M. O.; Ramakrisna, B. L.; Dreele, R. B. V. *J. Solid State Chem.* **1990**, *89*, 184.
(44) Brese, N. E.; O'Keefe, M. O.; VonDreele, R. B.; Young, V. G., Jr. *J. Solid State Chem.* **1989**, *83*, 1.
(45) Orgel, L. E. *J. Chem. Soc* **1958**, 4186.
(46) Müller-Buschbaum, H. *Z. Anorg. Allg. Chem.* **2004**, *630*, 2125.
(47) Lucier, G.; Münzeberg, J.; Casteel, W. J.; Bartlett, N. *Inorg. Chem.* **1995**, *34*, 2692.
(48) West, A. R. *Solid-State Electrochemistry*; Bruce, P. G., Ed.; Cambridge University Press: Cambridge, U.K., 1995; Chapter 2.